Enhanced and Correlated Lattice Vibrations of Relaxed Cu(001) Surface Studied by High-resolution Medium Energy Ion Scattering

Taishi Matsuda, Yuta Aiba, Jyunki Morimoto, Kei Mitsuhara, and Yoshiaki Kido*

Department of Physics, Ritsumeikan University, Kusatsu, Shiga-ken 525-8577, Japan

Abstract

The relaxed Cu(001) surface was analyzed by high-resolution medium energy ion scattering (MEIS) using 120 keV He^+ ions in a layer-by-layer fashion. We found the top-layer contraction of 1.6 % and the 2nd-layer expansion of 0.9 %, quite different from the close-packed (111) surface. Then enhanced thermal vibration amplitudes (TVAs) and the correlations between the 1st and 2nd nearest neighbor atoms in the [101]- and [001]-string were also determined simultaneously by MEIS spectrum analysis combined with Monte Carlo simulations of ion trajectories considering the surface relaxation and enhanced TVAs as well as correlations. We obtained the TVAs of the top-layer atoms strongly enhanced by 1.67±0.06 and 1.55±0.04 times that of the bulk (0.085 Å) in the lateral and surface normal direction, respectively and the correlation coefficients of +0.33±0.04 and +0.28±0.04, respectively for Cu atoms in the [101]- and [001]-axis oscillating perpendicular to each string. The correlation between the 2nd nearest neighbor atoms in the [101]-string is small probably less than +0.2. The results obtained here are compared with the other experimental reports and the Debye approximation as well as molecular dynamics simulations using the embedded atom method.

E-mail: ykido@se.ritsumei.ac.jp, Tel: +81-77-561-2710, Fax: +81-77-561-2657

I. INTRODUCTION

The (111) surface of a crystal taking a face-centered cubic lattice (fcc) is close packed and thereby most energetically stable. Therefore, another one such as (001) surface generally tends to be relaxed significantly and sometimes reconstructed to lower the surface energy. The Cu(001) has a typical relaxed surface without reconstruction. According to the previous investigations based on spectroscopic techniques[1-5] and theoretical calculations[6], the top inter-layer is contracted, while the 2nd inter-layer expanded. In addition, strong enhancements of the root-mean-square (rms) thermal vibration amplitudes (TVAs) take place in both lateral ($u_{//}$) and surface normal ($u_{\perp}$) directions compared with the bulk thermal vibration amplitude (u_{bulk}). So far, there are many reports on the enhanced thermal lattice vibrations of the Cu(001) surface[3-6]. For precise analysis, however, correlated thermal vibrations should be taken into account in any techniques. In many cases, however, the correlation effect has not been considered. Only the previous MEIS analysis[4] employed a simple reduction factor which takes account of the correlation effect to some extent. It is emphasized that the enhanced TVAs and correlations should be determined self-consistently.

Previously, we determined the top interlayer distance as well as enhanced and correlated thermal vibrations of the close-packed Cu(111) surface by high-resolution medium energy ion scattering (MEIS)[7]. It was revealed that the top interlayer distance is slightly contracted by 0.5 % and the thermal vibration amplitude in surface normal direction ($u_{\perp}$) is considerably enhanced by 70 %, while only slightly enhanced by 10 % in the lateral direction. The results presented above are in agreement with the molecular dynamics (MD) simulations using the embedded-atom method (EAM)[7]. However, the correlation coefficient determined by MEIS to be +0.24 is considerably smaller than that (+0.40) estimated from the MD simulations for the motion perpendicular to the [101]-string.

In this study, we determine precisely the top and 2nd inter-layer distances for Cu(001) by the shadowing effect resulting from a particle nature of medium energy He ions, which indeed makes shadow cones behind surface atoms. Monte Caro (MC) simulations of ion trajectories along some major crystal axes allow for calculating the close encounter (hitting) probability for each layer atoms taking account of the enhanced and correlated thermal vibrations. The enhanced TVAs of the top-layer atoms as well as the correlation coefficients between the 1st and 2nd nearest neighbor atoms

in the [101]- and [001]-string are determined in such a way that the MC simulation continues until the close encounter probabilities calculated from the simulation coincides with those derived from the observed MEIS spectrum. Therefore, it is essential to analyze the observed MEIS spectrum in a layer-by-layer manner and to employ a reliable line shape for each scattering component in order to decompose uniquely the observed MEIS spectra. The previous MEIS spectrum analysis[7] used asymmetric Gaussian shapes. It was found out later that the line shape for the scattering component from the top layer atoms was well reproduced by an exponentially modified Gaussian (EMG) profile[8,9]. This EMG line shape also reproduced well the MEIS spectra observed for Au nano-clusters[10,11]. Another important factor is the energy loss for ions incident and/or scattered along a major crystal axis. In this case, an ion passes close to a target nucleus and thus loses a large energy compared with random penetration, so called "skimming effect"[12]. Thus we take account of the skimming effect and employ the EMG function as the line shape to deconvolute the observed MEIS spectrum in the present analysis. The results obtained are compared with the theoretical predictions by the Debye approximation and the MD simulations employing the EAM potentials[13].

II. EXPERIMENTAL

Copper is a typical well conductive metal taking a fcc crystalline structure with a lattice constant of a = 3.615 Å (Debye temperature: Θ_D = 315 K)[14]. We purchased a disk-shaped and mirror-finished Cu(001) substrate with a purity of 4N from Surface Preparation Laboratory (SPL). The clean Cu(001) surface was prepared by many cycles of sputtering with 0.75-1.5 keV Ar^+ followed by annealing at 650°C for 10 min in ultrahigh vacuum (UHV) and then a (1×1) clear image was observed by reflection high energy electron diffraction (RHEED). No surface contaminations of C and O were confirmed by Auger electron spectroscopy and high-resolution MEIS. Then the sample was transferred to an UHV scattering chamber and mounted on a 6-axis goniometer. A 120 keV He^+ beam was incident on the sample surface and scattered He^+ ions were energy-analyzed by a toroidal electrostatic analyzer (ESA) with an energy resolution of $\Delta E / E \cong 1 \times 10^{-3}$ (full width at half maximum: FWHM)[15,16]. Such an excellent energy resolution allowing for layer-by-layer analysis was achieved mainly by making a well collimated beam size of 0.18 mm in the horizontal plane and a good spatial resolution of 40 μm of the position sensitive detector connected to the toroidal ESA.

The detection efficiency and the solid angle subtended by the toroidal ESA detector were ε = 0.44 and $\Delta\Omega$ = 7.64×10^{-5} [str], respectively. It is crucial to measure precisely an integrated beam current. For this purpose, the sample was positively biased by +90 V to suppress secondary electron emission and the beam current was conducted to ground via an ammeter. In order to avoid radiation damage to the sample surface, we shifted the beam position after accumulating a beam current of 1 μC.

Figure 1 shows a typical MEIS spectrum (circles) observed for 120 keV He^+ ions incident along the [$10\bar{1}$]-axis and backscattered to the [101]-direction. Two surface peaks clearly resolved correspond to the scattering components from two Cu isotopes, ^{63}Cu(69 %) and ^{65}Cu(31 %). The thick and thin solid curves, respectively are best-fitted total spectrum and decomposed scattering components from the top, 2nd- and 3rd-layer Cu atoms. Here, the energy differences between the scattering components from neighboring layers are ~2.0 times that for random penetration (skimming effect). The close encounter probabilities P_{CL} for the 2nd- and 3rd-layer Cu atoms are deduced to be 0.23±0.02 and 0.05±0.03, respectively by deconvoluting the surface peak. How to decompose the MEIS spectrum will be described later in detail.

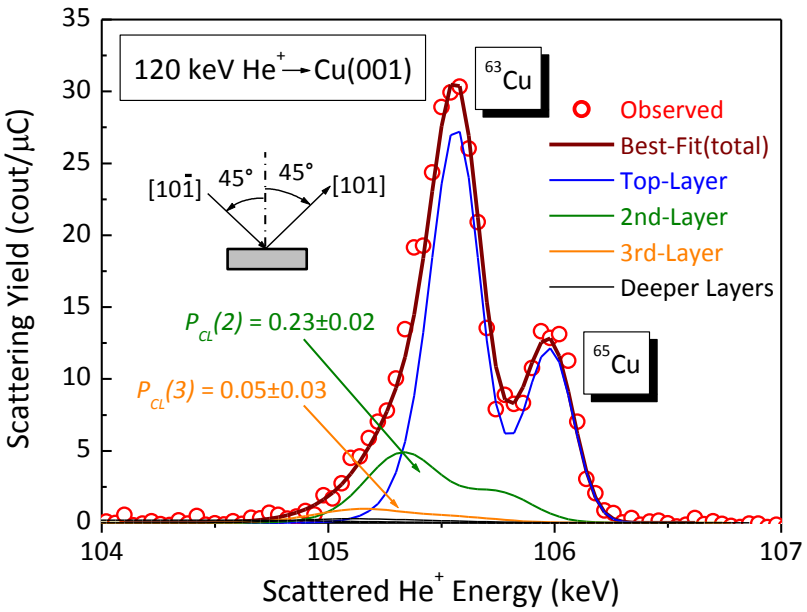

FIG.1. MEIS spectrum (circles) observed for 120 keV He^+ ions incident along the Cu-[$10\bar{1}$]-axis and scattered to 90° ([101]-axis). Thick and thin solid curves denote best-fitted total and decomposed spectra, respectively.

III. MONTE CARLO SIMULATIONS OF He ION TRAJECORIES

The scattering yield from the n-th layer atoms, Y_n is expressed by

$$Y_n(E_{out}(n)) = Q\,(d\sigma/d\Omega)\,N\Delta x\,\Delta\Omega\,\varepsilon\,\eta_+ P_{CL}(n)/\cos\theta_{in}, \quad (1)$$

where $E_{out}(n)$ is the emerging energy of He^+ ions scattered from the *n*-th layer atoms, *Q* number of incident He^+ ions, $d\sigma/d\Omega$ differential scattering cross section, $N\Delta x$ number of target atoms [atoms/cm^2] and η_+ is He^+ fraction. The close encounter probability for the *n*-th layer atoms is denoted by $P_{CL}(n)$ and θ_{in} is an incident angle with respect to surface normal. We employed the scattering cross sections proposed by Lee and Hart[17], which gives good approximations for relatively low Z-number atoms[18]. Indeed, for the scattering angle above 60° the Lee-Hart scattering cross sections agree well with those calculated from the Molière potential and also from the potential derived by solving the Poisson equation assuming the Hartree-Fock-Slater atomic model[19,20]. As mentioned before, in this MEIS spectrum analysis, we used the asymmetric line shape expressed by the EMG function, which was proposed by Grande et al.[8]. The EMG function is given by

$$f(E - E_{out}(n)) = \frac{1}{2\sigma_0} exp[-\frac{1}{2\sigma_0}\{2(E - E_{out}(n)) - \frac{\Omega_n^2}{\sigma_0}\}\{1 + erf(\frac{E - E_{out}(n) - \Omega_n{}^2/\sigma_0}{\sqrt{2}\Omega_n})\} \quad (2)$$

where σ_0 is an asymmetric parameter calculated by the coupled channel method[21,22] and Ω_n is the energy spread of emerging He^+ ions backscattered from the *n*-th layer atoms. The square of the energy spread is expressed by

$$\Omega_n^2 = \Omega_0^2 + \Omega_{LS}^2 N\,n\,d\{K^2/\cos\theta_{in} + 1/\cos\theta_{out}\} \quad (3)$$

where *N* and *d* are atomic number density and inter-atomic distance, respectively and *K* is a kinematic scattering factor. In the present case, the system energy resolution (standard deviation) is $\Omega_0 = 10^{-3} E_{out}^{(1)}/2.3548$. The energy straggling Ω_{LS} is given by the Lindhard-Scharff formula (*v*: ion velocity)[23],

$$\Omega_{LS}^2(E) = 0.5\times\{1.36\chi^{0.5} - 0.016\chi^{1.5}\}\times(4\pi\,Z_1^2 e^4 Z_2), \quad (\chi \equiv (v/v_B)^2/Z_2 \le 3)$$
$$v_B = 2.188\times10^8 \text{ [cm/s]} \quad e^2 = 14.40\times10^{-8} \text{ [eV cm]} \quad (4)$$

If the line shape and energy loss due to the skimming effect are given, the MEIS spectrum for He^+ ions scattered from the top layer atoms is uniquely synthesized. The reliability of the EMG line shape and the Lindhard-Scharff expression were confirmed

experimentally in advance[9,10,24,25]. Thus the exact line shape for each scattering component from the *n*-th layer atoms was given by the asymmetric factor derived from the coupled channel calculations and the energy spread calculated from the Lindhard-Scharff formula, as described before.

The enhanced TVAs of the top-layer atoms as well as correlations between the 1st and 2nd nearest neighbor atoms can be derived by calculating the close encounter probability, $P_{CL}(n)$ for each layer atoms. We performed the MC simulations of He ion trajectories based on the single-row approximation[26] and calculated the close encounter probabilities by varying the $u_{//}$ and $u_{\perp}$ values and the correlation coefficients until the calculated $P_{CL}(n)$ values coincide with the observed ones. Note that the close encounter probability is normalized by that for atoms undergoing no shadowing effect, for example, top-layer atoms. Figure 2 shows the schematic of a trajectory of an ion incident along some major crystalline axis. In the case of medium energy He^+ incidence, the time during passing through a lattice site atom is ~10^{-17} s, while the period of the thermal vibrations of Cu at room temperature (RT) is estimated to be ~2×10^{-14} s at least from the Debye cut-off frequency ($\omega_D = k_B\Theta_D/\hbar$; k_B: Boltzmann constant, $\hbar$: Planck constant). Therefore, the lattice site atoms can be regarded to be at rest during the passage of He ions.

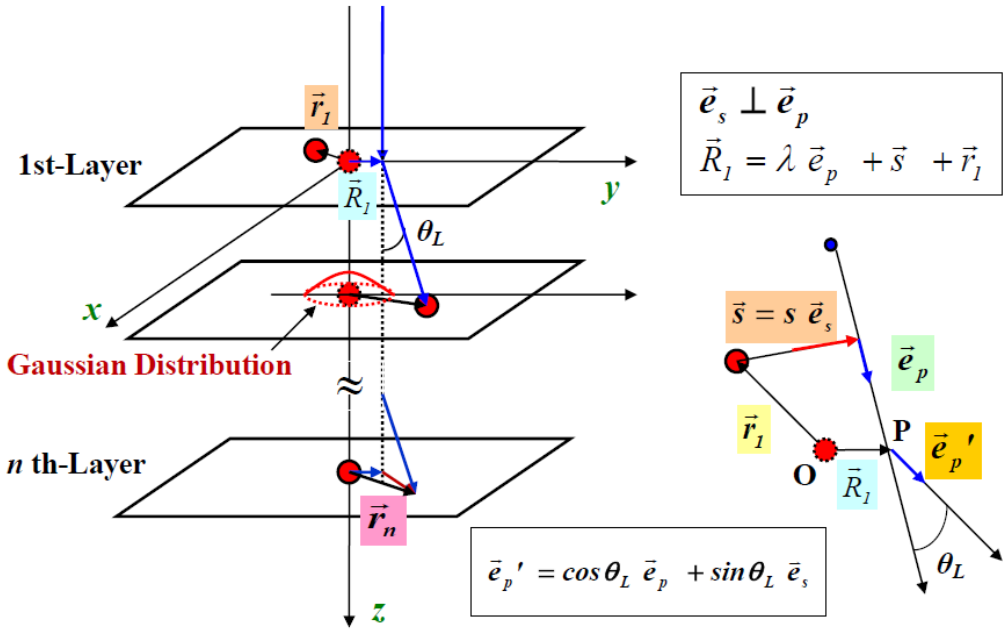

FIG.2. Ion trajectory along a string. The ion undergoes a series of small-angle collisions from thermally displaced lattice site atoms in the string.

The ion incident along a crystalline row taken as the *z*-axis undergoes a sequence of discrete small-angle deflections by the screened Coulomb potential of the atoms in the string. The incident position in the 1st layer is denoted as $\vec{R}_0 = (X_0, Y_0)$, which is generated by uniform random numbers. The position of the atom in the *n*-th layer $\vec{r}_n = \vec{r}_n^{\,/\!/} + \vec{r}_n^{\,\perp}$ (3D) is given taking account of the enhanced thermal vibration amplitudes and correlation coefficients assumed appropriately. A nuclear encounter would have taken place if the atom residing in the *n*-th layer were located exactly at $\vec{r}_n^{\,/\!/} = \vec{R}_n \ (\equiv \vec{R}_0 + \vec{\Delta}_n)$, where $\vec{R}_n : (X_n, Y_n)$ is the ion crossing position in the *n*th-layer. Note that only the coordinates in the (*x*, *y*) planes are relevant to the problem. The normalized close encounter (hitting) probability for the *n*th-layer atoms located in a crystal string (*z*-axis) is calculated by

$$
\begin{aligned}
P_{CL}(n) &= \int\!\!\ldots\!\int \varphi(\vec{r}_1, \vec{r}_2, \vec{r}_3, \ldots, \vec{r}_{n-1}, \vec{r}_0 + \vec{\Delta}_n)\, d^2\vec{r}_1 d^2\vec{r}_2 \ldots d^2\vec{r}_{n-1} d^2\vec{r}_0 \\
&= \int\!\!\ldots\!\int \varphi(\xi_1, \xi_2, \xi_3, \ldots, \xi_{2n-1}, \xi_{2n})\, d\xi_1 d\xi_2 d\xi_3 \ \ldots\ d\xi_{2n-1} d\xi_{2n} \\
&= Q \int\!\!\ldots\!\int \frac{\varphi(\xi_1, \xi_2, \ldots, \xi_{2n})}{q(\xi_1, \xi_2, \ldots, \xi_{2(n-1)})} \cdot \frac{q(\xi_1, \xi_2, \ldots, \xi_{2(n-1)})}{Q} d\xi_1 d\xi_2 \ldots d\xi_{2n} \\
&\cong \frac{Q}{N} \sum_{j=1}^{N} \frac{\varphi(\xi_1^{(j)}, \xi_2^{(j)}, \ldots, \xi_{2n}^{(j)})}{q(\xi_1^{(j)}, \xi_2^{(j)}, \ldots, \xi_{2(n-1)}^{(j)})}
\end{aligned}
\tag{5}
$$

$$
\xi_1 = \frac{x_1}{\sigma_x^{(1)}},\ \xi_2 = \frac{y_1}{\sigma_y^{(1)}},\ \ldots,\ \xi_{2n-3} = \frac{x_{n-1}}{\sigma_x^{(n-1)}}, \xi_{2n-2} = \frac{y_{n-1}}{\sigma_y^{(n-1)}},\ \xi_{2n-1} = \frac{X_n}{\sigma_x^{(n)}},\ \xi_{2n} = \frac{Y_n}{\sigma_y^{(n)}},
$$

where $\sigma_x^{(n)}$ is an rms one-dimensional (1D) TVA of the *n*th-layer atoms in the *x*-direction and $\vec{r}_j^{\,/\!/} \equiv (\vec{r}_1, \vec{r}_2, \ldots, \vec{r}_{n-1})$ is the correlated *2(n-1)*-dimensional position vector[26].

$$
\begin{aligned}
\varphi(\xi_1, \xi_2, \ldots, \xi_{2n}) &\equiv \frac{1}{\sqrt{(2\pi)^{2n} |S_{2n}|}} \exp\Big[-\frac{1}{2} \sum_{i=1}^{2n} \sum_{k=1}^{2n} (S_{2n}^{-1})_{ik}\, \xi_i\, \xi_k\Big] \\
q(\xi_1, \xi_2, \ldots, \xi_{2(n-1)}) &= \frac{1}{A} \frac{1}{\sqrt{(2\pi)^{2(n-1)} |S_{2(n-1)}|}} \exp\Big[-\frac{1}{2} \sum_{i=1}^{2(n-1)} \sum_{k=1}^{2(n-1)} (S_{2(n-1)}^{-1})_{ik}\, \xi_i\, \xi_k\Big] \\
Q &\equiv \int\!\!\ldots\!\int q(\xi_1, \xi_2, \ldots, \xi_{2(n-1)})\, d\xi_1 d\xi_2 \ldots d\xi_{2(n-1)} = 1
\end{aligned}
\tag{6}
$$

Here, *A* is an incident area, *N* the number of incident ions, and *S* is the correlation matrix given by $S_{ij} = \langle \xi_i \cdot \xi_j \rangle$, where < > means a time average. The $\xi \equiv (\xi_1, \xi_2, \ldots, \xi_{2(n-1)})$ is the correlated *2(n-1)*-variate normal distribution expressed by $\xi = T^{-1}\eta$, where $\eta \equiv (\eta_1, \eta_2, \ldots, \eta_{2(n-1)})$ is the normalized position vector generated

by assembling the normal distribution of the *2(n-1)*-univariate independent random variables and the transformation matrix T is given by $\tilde{T}T = S^{-1}$[27]. We assumed here no correlations between the *x* and *y* positions. We determine the enhanced TVAs of $u_{//}$ and $u_{\perp}$ and the correlation coefficients, S_{ij} in such a way that the assumed values reproduce the close encounter probabilities derived from the observed MEIS spectrum analysis.

The results obtained from the observed MEIS spectrum analysis combined with the MC simulations are compared with theoretical predictions calculated from the Debye model and the MD simulations using the EAM potential of the FBD (Foiles-Baskes-Daw) type[13]. The bulk TVA (u_{bulk}) and the correlation coefficients are simply expressed by the Debye approximation. The time-varied atomic displacement can be regarded as a wave function, which is expressed by superimposing the standing lattice waves as follows ($\vec{l}$: lattice vector):

$$\vec{u}(\vec{l}) = \sum_{\vec{q}}\sum_{\sigma}\left(\frac{\hbar}{2NM\omega_{q\sigma}}\right)^{1/2}\vec{e}_{q\sigma}\left[a_{q\sigma}\exp(i\vec{q}\cdot\vec{l}) + a^{+}{}_{q\sigma}\exp(-i\vec{q}\cdot\vec{l})\right], \tag{7}$$

where σ, $\vec{e}_{q\sigma}$ and $\omega_{q\sigma}$ represent a vibrational mode (longitudinal or transverse, acoustic or optical), the unit vector directed to wave vector $\vec{q}$ and the corresponding angular frequency of the mode, respectively. The atomic mass and atomic number density are denoted by *M* and *N*, respectively, and $a_{q\sigma}$ and $a^{+}_{q\sigma}$ are creation and annihilation operators satisfying the exchange relation. The derivation of the above expression is given in Appendix. The correlated vibration amplitude between the *n*-th nearest neighbor atoms is expressed as the following expectation value.

$$\begin{aligned}
&\langle\Phi|(\vec{u}(\vec{l})\cdot\vec{u}(\vec{l}+n\vec{d})|\Phi\rangle \\
&= \left(\frac{\hbar}{2NM}\right)\sum_{\vec{q}}\sum_{\sigma}\frac{1}{\omega_{q\sigma}}\langle\Phi|[a_{q\sigma}\exp(i\vec{q}\cdot\vec{l}) + a^{+}{}_{q\sigma}\exp(-i\vec{q}\cdot\vec{l})][a_{q\sigma}\exp\{i\vec{q}\cdot(\vec{l}+n\vec{d})\} + a^{+}{}_{q\sigma}\exp\{-i\vec{q}\cdot(\vec{l}+n\vec{d})\}]|\Phi\rangle \\
&= \left(\frac{\hbar}{2NM}\right)\sum_{\vec{q}}\sum_{\sigma}\frac{1}{\omega_{q\sigma}}\langle\Phi|a_{q\sigma}a^{+}{}_{q\sigma}\exp\{-in\vec{q}\cdot\vec{d}\} + a^{+}{}_{q\sigma}a_{q\sigma}\exp\{in\vec{q}\cdot\vec{d}\}|\Phi\rangle = \left(\frac{\hbar}{2NM}\right)\sum_{\vec{q},\sigma}\frac{1}{\omega_{\lambda}}(2n_{\lambda}+1)\cos[n\vec{q}\cdot\vec{d}] \\
&= \frac{\hbar}{M\Omega_{BZ}}\sum_{\sigma}\int\frac{1}{\omega_{\sigma}(\vec{q})}\left\{\frac{1}{\exp[\omega_{\sigma}(\vec{q})\hbar/k_{B}T]-1}+\frac{1}{2}\right\}\cos[n\vec{q}\cdot\vec{d}]\,d\vec{q}
\end{aligned} \tag{8}$$

where *d* and Ω_{BZ} are the inter-atomic distance in the string and the volume of the first Brillouin zone, respectively and the subscript λ denotes a (q, σ) mode. The correlated

thermal vibration amplitude for a monatomic crystal is given by

$$<\vec{u}(\vec{l})\cdot\vec{u}(\vec{l}+n\,\vec{d})>=\frac{6\pi\,\hbar}{M\Omega_{BZ}}\int_0^{q_D}\frac{q}{v}\{\frac{1}{exp(qv\,\hbar/k_BT)-1}+\frac{1}{2}\}\frac{2\sin(nd\,q)}{nqd}dq,\quad \frac{4\pi}{3}q_D^3=\Omega_{BZ} \tag{9}$$

where $v=(4\pi/3N)^{1/3}(k_B\Theta_D/2\pi\,\hbar)$. If one lets n = 0, the root-mean-square bulk thermal vibration amplitude (3D) is obtained. For Cu at RT, the Debye approximation gives the bulk thermal vibration amplitude of 0.084 Å. Figure 3 shows the correlation coefficients for the motion perpendicular to the [101]-string calculated from the MD simulations[7] and Debye model. The u_{bulk} value of 0.085 Å and the correlation coefficients for the nearest neighbors derived from the MD simulations coincide well with those calculated from the Debye approximation ($u_{bulk}=0.84$ Å), although slight deviations are seen for the nearest neighbor distance longer than $6\times\sqrt{2}a$.

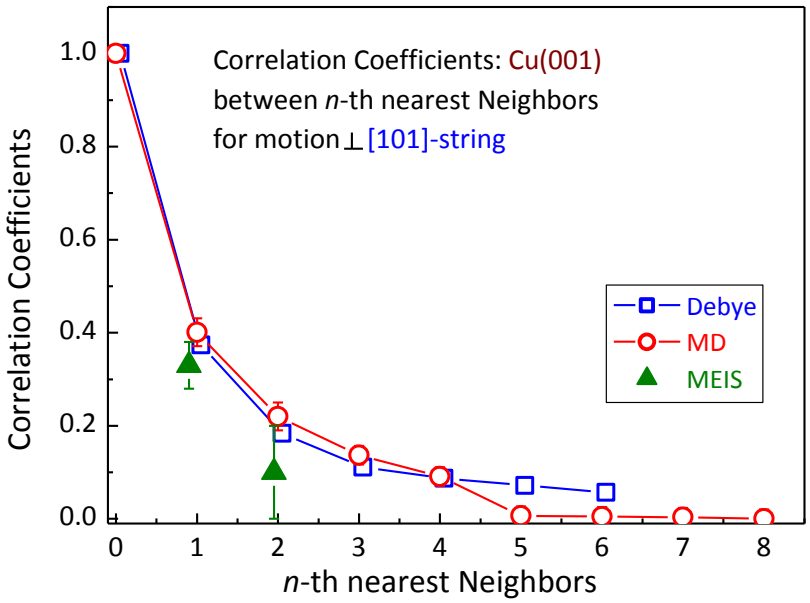

FIG.3. Correlation coefficients calculated from MD(open squares) and Debye model (full circles) for neighboring Cu atoms in the [101]-string for motion perpendicular to the [101]-axis. Triangles present MEIS results.

IV. RESULTS AND DISCUSSION

In the present study, we first determine the relaxed inter-layer distances and then estimate the enhanced TVAs and the correlation coefficients between the 1st and 2nd

nearest neighbor atoms in the [101]- and [001]-string for the motion perpendicular to the [101] and [001]-axis, respectively. To do that, MEIS spectra were measured for various scattering geometries, as indicated in Fig. 4. It is crucial to decompose precisely the observed MEIS spectrum into each scattering component from the top-down to 4th-layer atoms. The best-fit was obtained by the R-factor analysis, which is defined by

$$R \equiv \frac{\sum_i \{ \left| Y_j^{EXP}(E_i) - Y_j^{SIM}(E_i) \right| \cdot (Y_j^{EXP}(E_i)/Y_j^{Max}) \}}{\sum_i Y_j^{(EXP)}(E_i)} \qquad (10)$$

where $Y_j^{EXP}(E_i)$ and $Y_j^{SIM}(E_i)$, respectively are observed and simulated scattering yields for He^+ ions scattered from atomic species *j* with an energy E_i and Y_j^{Max} is the observed maximum yield for He^+ ions scattered from atoms *j* in the energy range of interest.

First we determine the relaxed interlayer distance between the top and 2nd-layer d_{12} and that between the 2nd- and 3rd-layer d_{23}. This can be made by a simple trigonometry for polar-angle scan profiles. We performed polar scans around (i) the $[10\bar{1}]$-axis at the [100]-azimuth and (ii) around the $[11\bar{2}]$-axis at the [110]-azimuth for 120 keV He^+ ions scattered mainly from the 2nd-layer atoms in the case of (i) and mainly from the 3rd- and 4th-layer atoms in the case of (ii) together with those scattered from deeper layer atoms (see Fig. 4 and Figs. 5(a) and (b)). In the case of (i), the angle giving a scattering yield minimum shifts by +0.46±0.05° from the [101]-axis for the scattering component mainly from the top-4th layers and that for the scattering component mainly from the 3rd-4th layers in the case of (ii) shifts by +0.1±0.05° from the [112]-axis. As the results, we obtain $d_{12} = 1.779 \pm 0.005$ and $d_{13} = 3.602 \pm 0.007$ Å and thus find the top-layer contraction of 1.6 % and the 2nd-layer expansion of 0.9 %. Such a surface relaxation found for the Cu(001) surface is quite pronounced compared with the slight contraction of 0.5 % for the (111) surface[7]. This result is consistent with the data given by the previous MEIS[3,4] and MD simulation[6] (see Table I).

Next, we derive the enhanced TVAs of the top-layer atoms in the lateral and surface normal directions. Hereafter, the MC simulations are performed considering the surface relaxation determined before (see Fig. 6). The root-mean-square bulk thermal vibration amplitude u_{bulk} was determined by taking a polar scan around the [001]-axis for scattering components from deeper layers. The simulated polar scan profile which

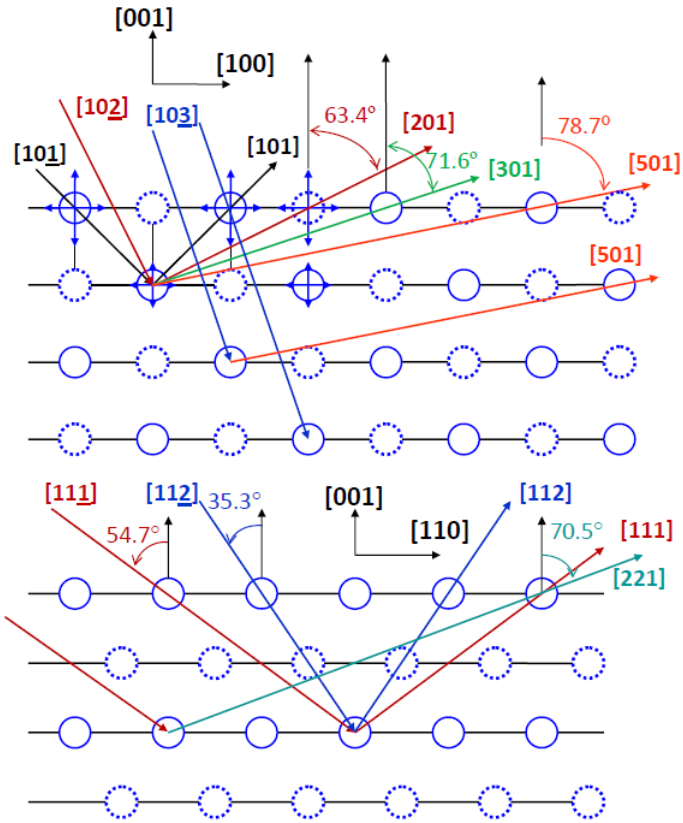

FIG.4. Side views of various scattering geometries in (010)- and ($1\bar{1}0$)-plane. Lattice site atoms denoted by solid circles and dashed circles belong to a different scattering plane.

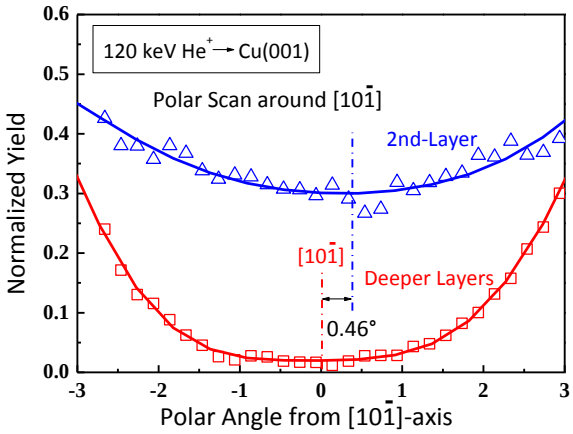

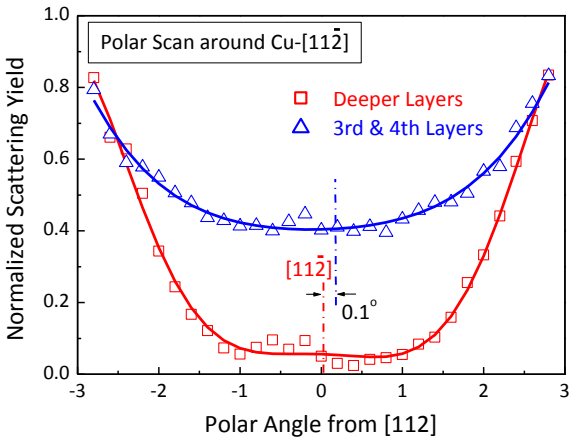

FIG.5. (a) Polar scan spectrum around [101]-axis observed for scattering components mainly from 2nd layer (triangles) and from deeper layers (circles). (b) Polar scan spectra around [$11\bar{2}$]-axis observed for scattering components mainly from 3rd and 4th layers (triangles) and from deeper layers (circles). Solid curves denote polynomial least square fitting.

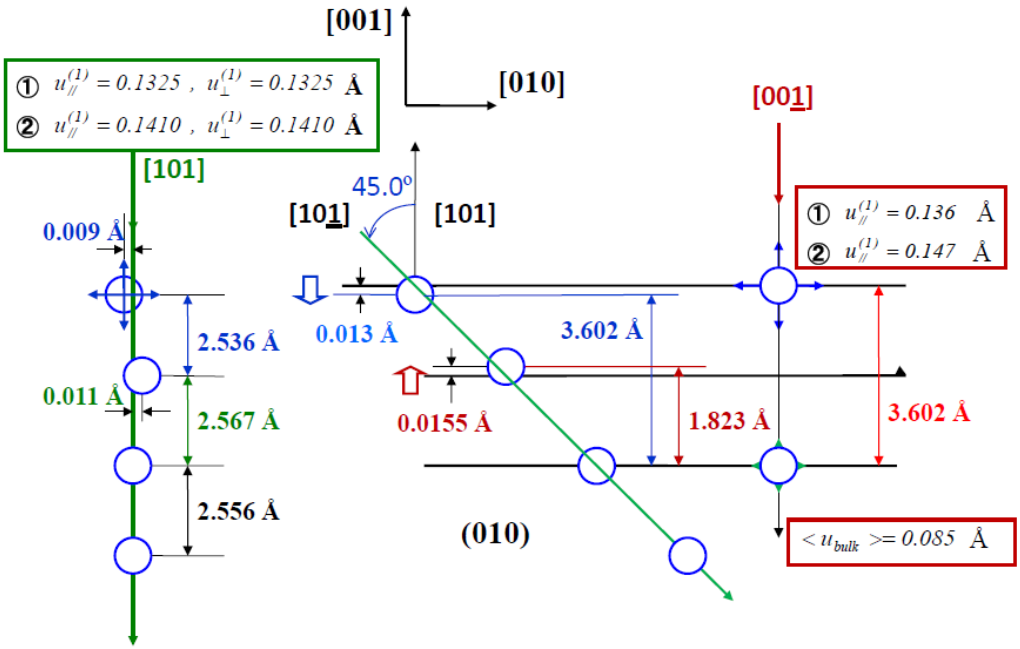

FIG.6. Side view of relaxed Cu(001) surface and [001]- and [101]-axis.

was obtained by calculating the close encounter probabilities for the atoms in the 7th-10th layers was best fitted to the observed one by assuming an appropriate u_{bulk} value. Figure 7 indicates the observed (squares) and simulated polar scan spectra as a function of polar angle around the [100]-axis. Obviously the assumption of $u_{bulk} = 0.085 \pm 0.003$ Å gives the best-fit, which coincides with the value of 0.085±0.002 Å calculated from the MD simulation and agrees well with the value of 0.084 Å derived from the Debye approximation.

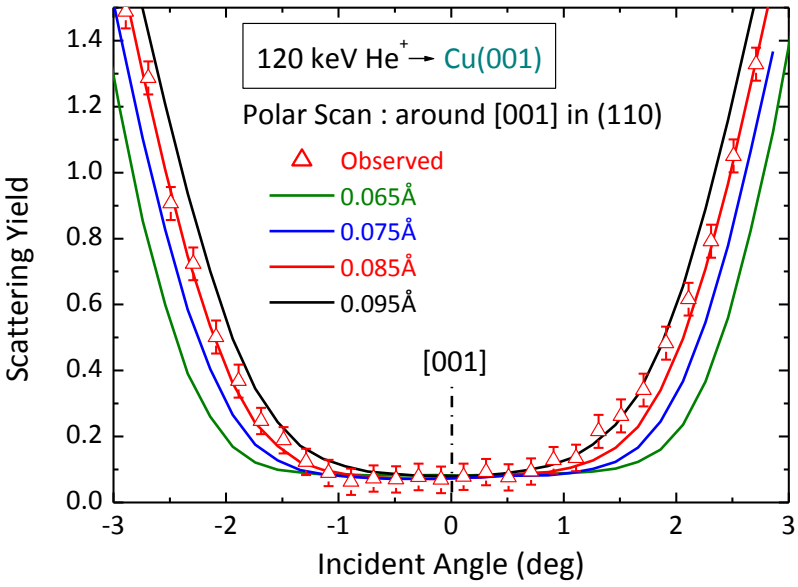

FIG.7. Observed polar scan spectrum (triangles) around [001]-axis in $(1\bar{1}0)$ plane for scattering component from deeper layers. Solid curves denote simulated polar scan profiles assuming 1D-thermal vibration amplitude of 0.065, 0.075, 0.085 and 0.095 Å.

We measured the following four MEIS spectra for 120 keV He^+ ions (i) (ii) incident along the $[11\bar{1}]$-axis and scattered to the [111]- and [221]-direction, (iii) the $[00\bar{1}]$-incidence and scattering to 81° about 3° off from the [100]-azimuth, and (iv) the $[10\bar{1}]$-incidence and scattering to the [101]-direction. In the case of (i) and (ii), $u_{//}^{(1)}$ and $u_{\perp}^{(1)}$ for top-layer atoms are the fitting parameters, which are determined by best-fitting both the surface peaks involving the scattering components from the top-, 2nd-, 3rd- and 4th-layer atoms. Note, here, that the top- and 2nd-layer atoms are not shadowed and the shadowing effect for the 3rd-layer atoms is quite the same as that for the 4th-layer atoms (see Fig. 4). The close encounter probabilities for the 3rd and 4th-layer atoms are deduced to be $P_{CL}^{111}(3,4)=0.30$ and $P_{CL}^{221}(3,4)=0.17$ for the ions passing along the [111]- and [221]-axis, respectively (The MEIS spectra are not shown here for brevity). Here, we assumed the approximation that the scattering event happening in the incident path is independent of that in the exit path and time reversibility[27] holds for the emerging path[27].

Figure 8(a) shows the combination of ($u_{//}^{(1)}$, $u_{\perp}^{(1)}$) which reproduces the close encounter probabilities for the 3rd- and 4th-layer atoms measured under the conditions (i) and (ii). The crossing point for the two curves gives the actual values of $u_{//}^{(1)}=0.136$ and $u_{\perp}^{(1)}=0.129$ Å (case (A)), respectively. Then we considered the correlations between the 1st nearest neighbor atoms in the [111]- and [221]-string (Debye: $S_{12}^{111}=+0.145$, $S_{12}^{221}=+0.079$) and calculated the combination of ($u_{//}^{(1)}$, $u_{\perp}^{(1)}$) which gives the same P_{CL} values deduced from the MEIS spectrum analysis and found $u_{//}^{(1)}=0.147$ and $u_{\perp}^{(1)}=0.135$ Å (case (B), see Fig. 8(b)), which are significantly larger by 7 % than those derived assuming no correlations. Here, we neglected enhancement of the TVAs of the 3rd- and 4th-layer atoms. If we consider the enhancement, the $u_{//}^{(1)}$ and $u_{\perp}^{(1)}$ values should be slightly reduced. In any case, the TVA for the atoms in the lateral direction is larger than that in the surface normal direction, quite different from the close-packed (111) surface[7]. This trend is consistent with the MD simulations[6] and previous MEIS analysis[4] (see Table I).

Then we determined the correlation coefficients between the 1st nearest neighbor atoms for the motion perpendicular to the [001]- and [101]-string from the close encounter probabilities derived by decomposing the MEIS spectra observed under the conditions of (iii) (see Fig. 9) and (iv). Assuming the time reversibility, the close encounter probability for the 2nd-layer atoms is deduced to be $\sqrt{0.23}=0.48$ (double alignment: $P_{CL}^2(2)=0.23\pm0.02$). Note that the correlation coefficients depend on the

TVAs of the atoms of interest. If we neglect the enhancement of the 2nd- and 3rd-layer atoms, we obtain $S_{12}^{001}=+0.19$ and $S_{12}^{101}=+0.25$ for the case (A) and $S_{12}^{001}=+0.24$ and $S_{12}^{101}=+0.31$ for the case (B). According to the MD simulations[6,7], the TVAs of the 2nd- and 3rd-layer atoms are also enhanced. Here, for simplicity we assume the same enhancement factors relative to the bulk TVA (0.085 Å) for the 2nd and 3rd-layer atoms calculated from the MD simulations ($u_{//}(2)=u_{\perp}(2)=0.102$ Å, $u_{//}(3)=u_{\perp}(3)=0.094$ Å). We estimated the correlation coefficients assuming the enhanced TVAs, as shown in Table II. If there is no enhancement for the TVAs for the 2nd- and 3rd-layer atoms, the $P_{CL}^{2}(3)$ value takes a much smaller value of 0.08×0.08 = 0.0064 than the observed one (0.05±0.03) for the case (iv) (see Fig. 1 and Table II).

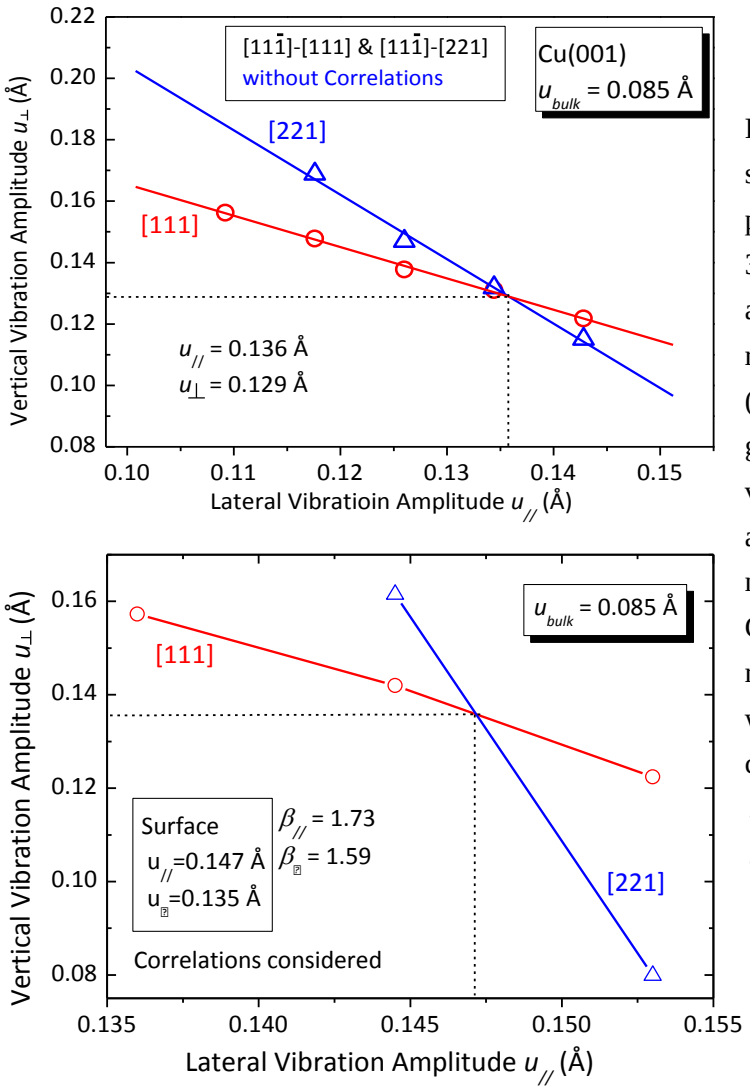

FIG.8 (a) Combination ($u_{//}^{(1)}$, $u_{\perp}^{(1)}$) satisfying the close encounter probabilities, 0.30 and 0.17 for the 3rd and 4th layer atoms for incident along the [111]- and [221]-axis, respectively. The crossing point ($u_{//}^{(1)}=0.136$, $u_{\perp}^{(1)}=0.129$ Å) gives just the real enhanced thermal vibration amplitudes of the top layer atoms. Calculations were made neglecting correlations. (b) Combination ($u_{//}^{(1)}$, $u_{\perp}^{(1)}$) reproducing the $P_{CL}(3,4)$ values, which was calculated assuming the correlation coefficients $S_{12}^{111}=+0.145$ for [111]-string and $S_{12}^{221}=+0.079$ for [221]-string.

This fact also suggests that it is reasonable to assume enhanced TVAs for the 2nd- and 3rd-layer atoms. As mentioned before, we neglected the enhancement of the TVAs for

the 3rd- and 4th-layer atoms, when derived the $u_{//}^{(1)}=0.147$ and $u_{\perp}^{(1)}=0.135$ Å. This reduces slightly the enhancement of TVAs for the top-layer atoms. So, we average the following three values for (i) $u_{//}^{(1)}=0.136$, $u_{\perp}^{(1)}=0.129$ Å and enhanced TVAs for the 2nd- and 3rd-layer atoms, (ii) $u_{//}^{(1)}=0.147$, $u_{\perp}^{(1)}=0.135$ Å and no enhancement for the 2nd- and 3rd-layer atoms, and (iii) $u_{//}^{(1)}=0.147$, $u_{\perp}^{(1)}=0.135$ Å and enhanced TVAs for the 2nd- and 3rd-layer atoms. Thus the most probable correlation coefficients are estimated to be $S_{12}^{001}=+0.28\pm0.04$ and $S_{12}^{101}=+0.33\pm0.04$. In the previous study[7], the correlation coefficient of $S_{12}^{101}=+0.24\pm0.05$ was deduced for Cu(111) surface, considerably smaller than that predicted by the Debye and MD simulation. This underestimate is attributed to neglecting the enhancement of the TVA for the 2nd-layer atoms. Finally, we tried to estimate the correlation coefficient for the 2nd nearest neighbor atoms in the [101]-string for the motion perpendicular to this axis. As

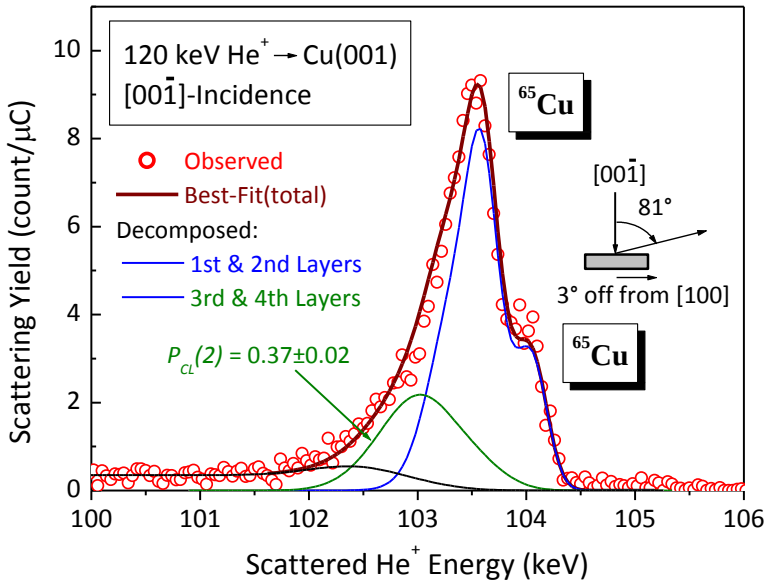

FIG.9. MEIS spectrum (circles) observed for 120 keV He^+ ions incident along the [$00\bar{1}$]-axis and scattered to 81° about 3° off from the [100]-azimuth (random direction). The thick solid curve is the best-fitted total spectrum assuming the close encounter probability of 0.37 for 3rd and 4th-layer atoms (equivalent). Thin solid curves correspond to decomposed spectra from (top + 2nd)-, (3rd + 4th)-, and deeper layers.

seen from Fig. 1, the $P_{CL}^{2}(3)$ for the [$10\bar{1}$]-incidence and scattering to the [101]-direction takes a very small value and has a large uncertainty. So, we measured the MEIS spectrum for He^+ ions incident 2.6° off from the [$10\bar{1}$]-axis at the [100]-azimuth (scattering angle was fixed to 90°), which is indicated in Fig. 10. Importantly, the MC simulations show that the $P_{CL}(2)$ is almost constant when one tilts

the incident beam direction from the [$10\bar{1}$]-axis within 3°, whereas the $P_{CL}(3)$ is significantly increased. The surface peak observed is decomposed into three scattering components from the top-, 2nd-, 3rd-layer atoms and background (from deeper layer atoms). Thus we obtained $P_{CL}^2(2)=0.27\pm0.03$ and $P_{CL}^2(3)=0.06\pm0.03$. The MEIS spectrum constructed without the contribution from the 3rd-layer is indicated by the thick dashed curve in Fig. 10. Note that the $P_{CL}^2(2)$(0.27) should be close to that (0.23)

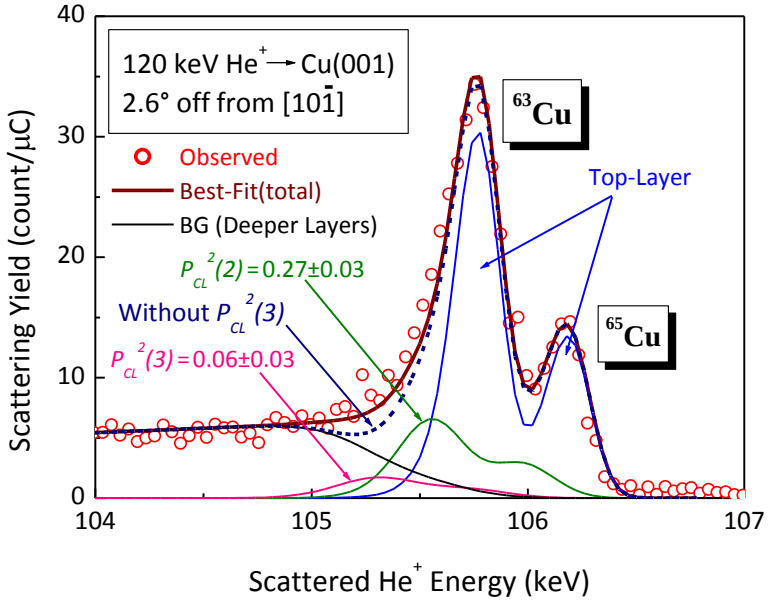

FIG.10. MEIS spectrum (circles) observed for 120 keV He^+ ions incident at 2.6° off from [$10\bar{1}$]-axis. Scattering plane and angle are (010) and 90°, respectively. Thick and thin solid curves are bet-fitted total spectrum and decomposed scattering components from 1st + 2nd (blue), 3rd + 4th (green), and deeper layers (black). Thick dashed curve is total spectrum without the scattering component from the 3rd-layer atoms.

observed for the double alignment geometry ([$10\bar{1}$]-incidence and [101]-emergence), as mentioned before. Obviously, there is a significant contribution from the 3rd-layer to the surface peak and this also suggests the enhanced TVAs for the 2nd- and 3rd-layer atoms (if not, the contribution is very small less than 0.01). As seen from Table II, it is difficult to determine exactly the correlation coefficient (S_{13}^{101}) between the second nearest neighbor atoms in the [101]-string, because the correlation between the 1st nearest neighbor atoms is a primary contribution to the close encounter probability. In addition, ambiguity in the enhanced TVAs for the 2nd- and 3rd-layer atoms increases the uncertainties in the close encounter probabilities. Considering the above uncertainties, the correlation coefficient S_{13}^{101} was estimated to be small probably less than +0.2 and larger than 0 (see Table II). Indeed, only acoustic phonons

appear for the crystalline lattice with one atom per primitive cell such as Cu and this mode leads to positive correlations. The correlation coefficients estimated here are basically consistent with the results calculated from the Debye approximation and MD simulations (see Fig. 3 and Table I).

Table I. Surface relaxation (+: expansion) and enhanced TVAs for top-layer atoms parallel ($u_{//}^{(1)}$) and perpendicular ($u_{\perp}^{(1)}$) to Cu(001) surface. Correlation coefficients between the first nearest neighbor atoms in the [001]- and [101]-string for the motion perpendicular to each axis, denoted by S_{12}^{001} and S_{12}^{101}, respectively. Correlation coefficient between the second nearest neighbor atoms in the [101]-string is denoted by S_{13}^{101}. All the data correspond to room temperature except for SXRD (160 K).

	Δd_{12} (%)	Δd_{23}	$u_{//}^{(1)}$ (Å)	$u_{\perp}^{(1)}$ (Å)	S_{12}^{001}	S_{12}^{101}	S_{13}^{101}
Present MEIS	−1.6±0.3	+0.9±0.3	0.142±0.005	0.132±0.003	+0.28±0.04	+0.33±0.04	< + 0.2
MEIS [3]	−2.4	+1	0.17	0.11			
MEIS [4]	−2.0	+1.0	0.147	0.136			
LEED [2]	−1.2	+0.9					
MD-EAM [6]	−1.21		0.114	0.113			
*SXRD [5]	−1.4±0.4	+0.3±0.4	0.109±0.015	0.118±0.025			
Debye					+0.22	+0.37	+0.18
MD-EAM [7]					+0.24	+0.40	+0.22

Table.II. Correlation coefficients and enhanced thermal vibration amplitudes (Å). The $P_{CL}(2)$ and $P_{CL}(3)$ values were derived from observed MEIS spectrum.($u_{bulk} = 0.085$ Å)

(i) Correlations for Cu atoms in the [101]-axis oscillating perpendicular to [101]-string.

Debye: S_{12}^{101} = +0.37, S_{13}^{101} = +0.184, MD: S_{12}^{101} = +0.40, S_{13}^{101} = +0.22, Present MEIS: $S_{12}^{101} = +0.33 \pm 0.04$

$u_{//}^{(1)}$	$u_{\perp}^{(1)}$	$u_{//}^{(2)}$	$u_{\perp}^{(2)}$	$u_{//}^{(3)}$	$u_{\perp}^{(3)}$	S_{12}^{101}	S_{13}^{101}	$P_{CL}(2)$ 0.48±0.03	$P_{CL}(3)$ 0.22±0.08
0.136	0.129	0.085	0.085	0.085	0.085	0.25	0	0.48	0.08
0.136	0.129	0.102	0.102	0.094	0.094	**0.32**	0	0.48	0.12
0.147	0.135	0.085	0.085	0.085	0.085	**0.31**	0	0.48	0.08
0.147	0.135	0.102	0.102	0.094	0.094	**0.37**	0	0.48	0.11
0.147	0.135	0.102	0.102	0.094	0.094	0.37	0.1	0.48	0.10
0.147	0.135	0.102	0.102	0.094	0.094	0	0	0.67	0.21

V. CONCLUSION

High-resolution MEIS analysis for the Cu(001) surface revealed the top-layer contraction of 1.6 % and the 2nd-layer expansion of 0.9 %. This result is consistent with the results of previous MEIS[3,4], LEED[2] and MD simulation[6]. We determined the bulk TVA to be 0.085±0.003 Å, which is in good agreement with that calculated from the Debye approximation (0.084 Å) and from the MD using the EAM

potential (0.085 Å). Then we derived the TVAs for the top-layer atoms in both lateral and surface normal directions, strongly enhanced by 67 % and 55 % (averaged for two cases), respectively, which are consistent with the results of the previous MEIS[4], while significantly larger than those calculated from the MD[6]. Interestingly, the enhancement in the lateral direction is larger than that in surface normal direction, quite different from the close-packed Cu(111) surface[7]. In addition, significant enhancement also occurs for the 2nd- and 3rd-layer atoms, which should be taken into account to determine correlation coefficients. Considering the surface relaxation and enhanced thermal vibrations for the subsurface atoms, we estimated the correlation coefficients between the 1st nearest neighbor atoms to be +0.28±0.04 and +0.33±0.04 for the motion perpendicular to the [001]- and [101]-string, respectively. The correlation coefficient between the 2nd-nearest neighbor atoms in the [101]-string was estimated to be small probably less than +0.2. The results of correlation coefficients obtained here are basically consistent with the MD simulations and Debye approximation.

(ii) Incidence 2.6° off from [101]-axis.

$u_{//}^{(1)}$	$u_{\perp}^{(1)}$	$u_{//}^{(2)}$	$u_{\perp}^{(2)}$	$u_{//}^{(3)}$	$u_{\perp}^{(3)}$	S_{12}^{101}	S_{13}^{101}	$P_{CL}(2)$ 0.51±0.04	$P_{CL}(3)$ 0.024±0.07
0.147	0.135	0.102	0.102	0.094	0.094	0	0	0.68	0.26
0.147	0.135	0.102	0.102	0.094	0.094	0.33	0	0.51	0.16
0.147	0.135	0.102	0.102	0.094	0.094	0.33	0.10	0.51	0.15
0.147	0.135	0.102	0.102	0.094	0.094	0.33	0.20	0.51	0.14
0.147	0.135	0.102	0.102	0.094	0.094	0.33	0.30	0.51	0.12

(iii) Correlations for Cu atoms in the [001]-axis oscillating perpendicular to [001]-string.

Debye: $S_{12}^{001} = +0.22$, MD: $S_{12}^{001} = +0.24$, Present MEIS: $S_{12}^{001} = +0.28 \pm 0.04$

$u_{//}^{(1)}$	$u_{\perp}^{(1)}$	$u_{//}^{(2)}$	$u_{\perp}^{(2)}$	$u_{//}^{(3)}$	$u_{\perp}^{(3)}$	S_{12}^{001}	$P_{CL}(2)$: 0.37±0.03
0.136	0.129	0.085	0.085	0.085	0.085	0.19	0.37
0.136	0.129	0.102	0.102	0.094	0.094	**0.28**	0.37
0.147	0.135	0.085	0.085	0.085	0.085	**0.24**	0.37
0.147	0.135	0.102	0.102	0.094	0.094	**0.32**	0.37
0.147	0.135	0.102	0.102	0.094	0.094	0	0.60

ACKNOWLEDGMENTS

The authors would like to appreciate K. Tominaga for calculating the correlation coefficients based on the Debye model.

References

[1] H.L. Davis and J.R. Noonan, Surf. Sci. **126** (1983) 245.

[2] D.M. Lind, F.B. Dunning, G.K. Walters and H.L. Davis, Phys. Rev. **B 35** (1987) 9037.

[3] Q.T. Jiang, P. Fenter and T. Gustafsson, Phys. Rev. **B 44** (1991) 5773.

[4] D.E. Fowler and J.V. Barth, Phys. Rev. **B 52** (1995) 2117.

[5] O. Mirionets, H.L. Meyerheim, C. Tusche, P. Zschack, H. Hong, J. Jeutter, R. Felici and J. Kirschner, Phys. Rev. **B 78** (2008) 153401.

[6] L. Yang, T.S. Rahman and M.S. Daw, Phys. Rev. **B 44** (1991) 13725.

[7] T. Okazawa, F. Takeuchi and Y. Kido, Phys. Rev. **B 72** (2005) 075408.

[8] P.L. Grande, A. Hentz, R.P. Pezzi, I.J.R. Baumvol, and G. Schiwietz, Nucl. Instrum. Methods **B 256** (2007) 92.

[9] M. Hazama, Y. Kitsudo, T. Nishimura, Y. Hoshino, P.L. Grande, G. Schiwietz and Y. Kido, Phys. Rev. **B 78** (2008) 194302.

[10] H. Matsumoto, K. Mitsuhara, A. Visikovskiy, T. Akita, N. Toshima and Y. Kido, Nuclear Instruments and Methods **B 268** (2010) 2281.

[11] M.A. Sortica, P.L. Grande. G. Machado, and L. Miotti, J. Appl. Phys. **106** (2009) 114320.

[12] K. Mitsuhara, T. Matsuda, K. Tominaga, P.L. Grande, G. Schiwietz, and Y. Kido, Phys. Rev. **A** in press.

[13] S.M. Foiles, M.I. Baskes and M.S. Daw, Phys. Rev. **B 33** (1986) 7983.

[14] D.S. Gemmell, Rev. Mod. Phys. **46** (1974) 129.

[15] T. Nishimura, A. Ikeda and Y. Kido, Rev. Sci. Instrum. **69** (1998) 1671.

[16] Y. Kido, T. Nishimura, Y. Hoshino and H. Namba, Nucl. Instrum. Methods **B 161-163** (2000) 371.

[17] S.R. Lee & R.R. Hart, Nucl. Instrum. Methods **B 463-467** (1993) 463.

[18] T. Nishimura, K. Mitsuhara, A. Visikovskiy and Y. Kido, Nucl. Instrum. Methods **B 280** (2012) 5.

[19] E. Clementi and C. Roetti, Atomic and Nucl. Data Tables **14** (1974) 177.

[20] A.D. McLean and R.S. McLean, Atomic and Nucl. Data Tables **26** (1981) 197.
[21] G. Schiwietz, Phys. Rev. **A 42** (1990) 296.
[22] P.L. Grande and G. Schiwietz, Nucl. Instrum. Methods **B 132** (1997) 264.
[23] J. Lindhard and M. Scharff, K. Dan. Vidensk. Selsk. Mat. Fys. Medd. **27**, no.15 (1953).
[24] Y. Kido and T. Koshikawa, Phys. Rev. **A 44** (1991) 1759.
[25] K. Mitsuhara, H. Okumura, T. Matsuda, M. Tagami, A. Visikovskiy and Y. Kido, Nucl. Instrum. Methods **B 276** (2012) 56.
[26] J.F. Ziegler, J.P. Biersack, and W. Littmark, *The Stopping and Range of Ions in Matter* (Pergamon, New York, 1985).
[27] J.F. van der Veen, Surf. Sci. Rep. **5** (1985) 199.
[28] D.P. Jackson and J.H. Barrett, Computer Phys. Commun. **13** (1977) 157.

Appendix

For simplicity, first we consider one dimensional and periodic atomic (mass: *M*) chain with a length of $L = Na$ where a and N are an inter-atomic distance and number of atoms, respectively. The equation of motion for the n-th atom is given by

$$M\frac{d^2\xi_n}{dt^2} = \kappa\{(\xi_{n+1} - \xi_n) - (\xi_n - \xi_{n-1})\}, \tag{1}$$

where $\xi_n(t)$ is a displacement of the atom and κ is a spring constant. Of course, $\xi_n(t)$ satisfies the periodic condition, $\xi_{n+N}(t) = \xi_n(t)$. Then the $\xi_n(t)$ can be expanded by lattice Fourier series.

$$\xi_n(t) = \frac{1}{\sqrt{N}}\sum_q \xi_k(t) exp(i\, qx_n) \quad (\xi_{-q} = \xi_q^*,\ x_n = na) \tag{2}$$

The inverse Fourier transform is written by

$$\xi_q(t) = \frac{1}{\sqrt{N}}\sum_n \xi_n(t) exp(-i\, qx_n). \tag{3}$$

Here, we note that $\sum_q exp\{i\, qa(m-n)\} = N\delta_{m\,n}$. The equation of motion for $\xi_q(t)$ is expressed by

$$\frac{d^2\xi_q}{dt^2} + \frac{\kappa}{M}\{1 - cos(qa)\}\xi_q = 0. \tag{4}$$

Then we obtain the solution of $\xi_q(t)=\xi_q\, exp(-i\omega_q t)$ and the dispersion relation $\omega_q=\sqrt{\frac{2\kappa}{M}\{1-cos(qa)\}}$ for acoustic phonon. Next, we introduce a canonical momentum for ξ_q defined as $\pi_q = M\frac{d\xi_{-q}}{dt}$ and expand $\pi_n(t)$ by Fourier series.

$$\pi_n(t)\equiv M\frac{d\xi_n}{dt}=\frac{M}{\sqrt{N}}\sum_q\frac{d\xi_q}{dt}exp(i\ qx_n)=\frac{M}{\sqrt{N}}\sum_q\frac{d\xi_{-q}}{dt}exp(-i\ qx_n)=\frac{M}{\sqrt{N}}\sum_q\pi_q\, exp(-i\ qx_n) \tag{5}$$

Thus the Hamiltonian is written by

$$H=\frac{1}{2M}\sum_n\pi_n^2+\frac{\kappa}{2}\sum_n(\xi_{n+1}-\xi_n)^2=\frac{1}{2M}\sum_q\pi_q\pi_{-q}+\frac{M}{2}\sum_q\omega_q^2\xi_q\xi_{-q} \tag{6}$$

In order to quantize the lattice wave, we must introduce a continuum variable *x* instead of x_n. This can be done by taking a limitation that $a\to 0$.

The quantization of the lattice wave is made by introducing the following commutation relation,

$$[\xi_m,\ \pi_n]\equiv\xi_m\pi_n-\pi_n\xi_m=i\,\hbar\delta_{m\,n} \tag{7}$$

Then the Fourier components satisfy the following commutation relation,

$$[\xi_q,\ \pi_\rho]=\frac{1}{N}\sum_m\sum_n[\xi_m,\ \pi_n]\,exp(i\ qx_m)exp(-i\ \rho x_n)=\frac{i}{N}\sum_m exp\{i\ (q-\rho)am\}=i\hbar\delta_{q\,\rho} \tag{8}$$

Now we introduce creation ($\hat{a}^+$) and annihilation ($\hat{a}$) operators defined by

$$a_q\equiv\sqrt{\frac{1}{2\hbar\ M\omega_q}}(M\omega_q\xi_q+i\ \pi_{-q}),\ \ a_q^+\equiv\sqrt{\frac{1}{2\hbar\ M\omega_q}}(M\omega_q\xi_q^+-i\ \pi_{-q}^+). \tag{9}$$

This leads to $[a_q,\ a_\rho^+]=\delta_{q\,\rho}$ (10)

Here, we note that $\xi_q^+=\xi_{-q}$ and $\pi_q^+=\pi_{-q}$.

Thus the Hamiltonian is represented by $H=\sum_q\omega_q\hbar\ (a_q^+a_q+\frac{1}{2})$ (11)

From eq. (9), we have $\xi_q=\sqrt{\frac{\hbar}{2M\omega_q}}(a_q+a_{-q}^+),\ \ \pi_q=-i\sqrt{\frac{M\omega_q\hbar}{2}}(a_{-q}-a_q^+)$ (12)

Finally, the following expression is obtained:

$$\xi_n=\frac{1}{\sqrt{N}}\sum_q\sqrt{\frac{\hbar}{2M\omega_q}}(a_q+a_{-q}^+)exp(iqx_n)=\sum_q\sqrt{\frac{\hbar}{2NM\omega_q}}\{a_q\,exp(iqx_n)+a_q^+\,exp(-iqx_n)\} \tag{13}$$

This one dimensional form is easily generalized to three dimensional expression,

$$\vec{u}(\vec{l}\,) = \sum_{\vec{q}}\sum_{\sigma}\sqrt{\frac{\hbar}{2NM\omega_{q\sigma}}}\vec{e}_{q\sigma}\{\, a_{q\sigma}\, exp(\, i\vec{q}\cdot\vec{l}\,) + a^{+}_{q\sigma}\, exp(\, -i\vec{q}\cdot\vec{l}\,)\}, \tag{14}$$

where N and σ corresponds to atomic number density and three acoustic modes of longitudinal (one) and transverse (two) lattice waves, respectively and $\vec{e}_{q\,\sigma}$ denotes the unit vector. The practical physical value of the displacement of a lattice site atom is given as an expectation value given by $\langle \Phi | (\vec{u}(\vec{l}\,)\cdot\vec{u}(\vec{l}+n\vec{d}\,)) | \Phi \rangle$, (15)

where $\langle \Phi |$ corresponds to a quantized crystalline phonon field. Substituting eq.(15) into eq.(14) leads to

$$\begin{aligned}
&\langle \Phi | (\vec{u}(\vec{l}\,)\cdot\vec{u}(\vec{l}+n\vec{d}\,)) | \Phi \rangle \\
&= (\frac{\hbar}{2NM})\sum_{\vec{q}}\sum_{\sigma}\frac{1}{\omega_{q\sigma}}\langle \Phi | [\, a_{q\sigma}\, exp(\, i\vec{q}\cdot\vec{l}\,) + a^{+}{}_{q\sigma}\, exp(\, -i\vec{q}\cdot\vec{l}\,)][\, a_{q\sigma}\, exp\{\, i\vec{q}\cdot(\vec{l}+n\vec{d}\,)\} + a^{+}{}_{q\sigma}\, exp\{\, -i\vec{q}\cdot(\vec{l}+n\vec{d}\,)\}] | \Phi \rangle \\
&= (\frac{\hbar}{2NM})\sum_{\vec{q}}\sum_{\sigma}\frac{1}{\omega_{q\sigma}}\langle \Phi | a_{q\sigma}a^{+}{}_{q\sigma}\, exp\{\, -in\vec{q}\cdot\vec{d}\,\} + a^{+}{}_{q\sigma}a_{q\sigma}\, exp\{\, in\vec{q}\cdot\vec{d}\,\} | \Phi \rangle \\
&= (\frac{\hbar}{2NM})\sum_{\vec{q},}\sum_{\sigma}\ \frac{1}{\omega_{q\,\sigma}}(\, 2n_{q\,\sigma}+1)\cos[\, n\vec{q}\cdot\vec{d}\,]
\end{aligned} \tag{16}$$

Here, $\langle n_{q\,\sigma} | a_{q\,\sigma}a^{+}_{q\,\sigma} | n_{q\,\sigma} \rangle = n_{q\,\sigma}$ and $\langle n_{q\,\sigma} | a^{+}_{q\,\sigma}a_{q\,\sigma} | n_{q\,\sigma} \rangle = n_{q\,\sigma}+1$ are used ($\langle \Phi | \rightarrow \langle n_{q\,\sigma} |$). If one assumes a thermal equilibrium at a temperature of T K, the time averaged number of the phonon (q, σ) is given by Bose-Einstein statistics.

$$< n_{q\,\sigma}(T) > = \frac{1}{exp[\, \omega_{\sigma}(\vec{q}\,)\hbar / k_B T\,] - 1} \tag{17}$$